Computer Simulation of Incommensurate Diffusion in Zeolites: Understanding Window Effects

David Dubbeldam* and Berend Smit

Department of Chemical Engineering, University of Amsterdam, Nieuwe Achtergracht 166, 1018 WV Amsterdam, The Netherlands

Received: May 3, 2003

Dedicated molecular simulation techniques afford the study of the abnormal adsorption and diffusion of linear alkanes in ERI-, CHA-, and LTA-type zeolites. The exceptionally slow diffusion rates required the development of a combination of rare-event transition-state theory techniques and the configurational-bias Monte Carlo algorithm. The diffusion coefficients computed by this novel method agree well with the nondisputed rates determined experimentally for LTA-type sieves. The computed rates corroborate the nonmonotonic variation of the diffusion rate with alkane chain length published by Gorring, that is, the rate increases by orders of magnitude when the molecular and cage shape are no longer commensurate, so a molecule ends up stretched across a cage tethered at opposite windows. The simulations corroborate this "window effect" for both ERI- and CHA-type sieves and suggest that it is characteristic for all sieves with windows approximately 0.4 nm across. They predict that it also occurs for LTA-type sieves provided that the *n*-alkane is long enough to exceed the diameter of the LTA-type supercage.

I. Introduction

With the potential substitution of methyltertiarybutyl ether (MTBE) by ethanol in gasoline, it will be difficult to maintain gasoline volatility without removing a substantial amount of the volatile pentanes together with the MTBE. In the 1960s, the selective hydrocracking of pentanes and hexanes under reforming conditions was commercialized using a catalyst based on an ERI-type zeolite.[1] One could envisage a resurgence of such a process if the catalyst could somehow be reformulated so as to exhibit a higher selectivity for pentane removal than the ERI-type zeolite. An impediment to such a development is that the fundamental operating principles of the ERI-type zeolite have never been fully understood at a molecular level. This paper attempts to remedy this situation by applying state of the art molecular simulation techniques to assess the catalytically relevant diffusion and adsorption phenomena.

In 1973, Gorring reported an experimental study of diffusion of several *n*-alkanes over zeolite T.[2] Zeolite T is a disordered intergrowth of OFF- and ERI-type zeolites: the OFF-type structure consists of channels 0.67 nm across; the ERI-type structure of cages is linked by a highly tortuous diffusion path through 0.4 nm windows. Surprisingly, the diffusion and reaction rates in ERI-type zeolites reportedly increase significantly going from *n*-C_8 to *n*-C_{12} before the usual monotonic decrease with alkane chain lengths sets in. According to Gorring[2] and Chen,[3,4] the diffusion rate exhibits a maximum for *n*-C_{12} because the shape is incommensurate with that of an ERI-type cage, so that *n*-C_{12} is always inside an ERI-type window. Smaller molecules are commensurate with the ERI-type cage and remain trapped in its potential well. Larger molecules also gain stability from the interactions with the cage. Gorring argued that the occurrence of the window effect might be a general phenomenon common to diffusion of long molecules in many zeolites, the position of minima and maxima being determined by identifiable crystal parameters.

The origin of the window effect is a relatively unfavorable adsorption for the chain lengths close to the cage size combined with a low orientational freedom as the chains are stretched across a cage tethered at opposite windows.[5,6] As the movement of the incommensurated chain is less impeded by the higher free energy barriers a commensurated chain would feel, it has an enhanced mobility around integer values of the ratio of the chain length to the period of a lattice. Perhaps the simplest model for molecules that are either commensurate or incommensurate with the framework structure is the 1938 Frenkel−Kontorowa (FK) model[7,8] for adsorbed atoms on a periodic substrate. The model, consisting of a string of atoms connected by springs and subjected to a periodic potential, contains for a vanishing potential a "floating phase" that is incommensurate for almost all values of the ratio a/b, where a is the equilibrium lattice spacing of the harmonic chain and b is the lattice period. Similar models have been proposed by Ruckenstein and Lee,[9] Derouane et al.,[10] and Nitsche and Wei.[11] However, we are aware neither of theoretical studies closer to reality nor of additional experimental confirmation of the nonmonotonic variation of diffusion with alkane chain length. On the contrary, recent attempts[12,13] failed to corroborate Gorring's diffusion data.

An intensive research effort on measuring diffusion rates in zeolites augmented the number of techniques to measure the diffusion rates, and the discrepancies between the rates obtained by the various methods. Thus, agreement among microscopic (pulsed field gradient NMR, quasi-elastic neutron scattering), mesoscopic (micro-FTIR), and macroscopic (membrane permeation, uptake methods, zero-length column, frequency response) techniques is rare. As compared to Cavalcante et al.[12] and Magalhães et al.,[13] Gorring used too much sample in his mass uptake measurements and changed his sorbate concentration too drastically, so his data were prone to the intrusion of heat transfer and extracrystalline mass-transfer phenomena. The discrepancy between the experiments motivated us to develop a molecular simulation method that would allow us to study the adsorption and diffusion and shed some light on the

* Corresponding author. E-mail: dubbelda@science.uva.nl.

10.1021/jp035200m CCC: $25.00
Published on Web 10/11/2003

experimental dispute. Furthermore, we hope to contribute valuable new insights to the theory of diffusion in zeolites.

In this paper, we use configurational-bias Monte Carlo (CBMC) to obtain the Henry coefficients and heats of adsorption in OFF-, ERI-, CHA-, and LTA-type silica. We apply the transition-state theory (TST) Bennet−Chandler approach[14,15] and the techniques developed by Ruiz-Montero et al.,[16] combined with CBMC, to calculate diffusion coefficients in ERI-type, CHA-type, and LTA-type silica. Both Henry coefficients and diffusion coefficients are calculated over a wide range of chain lengths and temperatures. The diffusion data are fitted with an Arrhenius law producing activation energies and frequency factors. For ERI- and CHA-type sieves, we confirm the existence of the window effect. The physical origin of the window effect and the conditions under which the phenomenon occurs are studied in detail.

The remainder of this paper is organized as follows. First, we introduce our simulation model in section II and review the relevant theoretical foundations in section III. Next we discuss the choice of the reaction coordinate needed in the transition-state theory in section IV. A detailed description of the zeolites is presented in section V. In section VI, simulation results on adsorption, diffusion, activation energies, and frequency factors are reported, and we discuss the comparison with the scattered experimental results. We discuss the comparison with some theoretical and experimental results in section VII and end in section VIII with some concluding remarks.

II. Simulation Model

We use the united atom model[17] and consider the CH_3 and CH_2 groups as single interaction centers with their own effective potentials. The pseudoatoms in the chain are connected by harmonic bonding potentials. Bond bending among neighboring pseudoatoms *i*, *j*, and *k* is modeled by a harmonic cosine bending potential, and changes in the torsional angle are controlled by a Ryckaert−Bellemans potential.[18] The pseudoatoms in different molecules, or belonging to the same molecule but separated by more than three bonds, interact with each other through a shifted Lennard-Jones potential.

In the CBMC scheme, it is convenient to split the total potential energy of a trial site into two parts. The first part is the internal, bonded potential, U^{int}, which is used for the generation of trial orientations. The second part of the potential, the external potential (U^{ext}), is used to bias the selection of a site from the set of trial sites. Note that the split can be made completely arbitrarily. The internal energy U^{int} is given by

$$U^{\text{int}} = U^{\text{bond}} + U^{\text{bend}} + U^{\text{torsion}} \tag{1}$$

with

$$U^{\text{bond}} = \sum_{\text{bonds}} \frac{1}{2} k_1 (r - r_0)^2 \tag{2}$$

$$U^{\text{bend}} = \sum_{\text{bends}} \frac{1}{2} k_2 (\cos\theta - \cos\theta_0)^2 \tag{3}$$

$$U^{\text{torsion}} = \sum_{\text{torsions}} \sum_{n=1}^{6} C_n \cos^n \phi \tag{4}$$

where $k_1/k_B = 96\,500$ K/Å^2 is the bond force constant, $r_0 = 1.54$ Å is the reference bond length, $k_2/k_B = 62\,500$ K/rad^2 is the bend force constant, $\theta_0 = 114°$ is the reference bend angle, and ϕ is the dihedral angle (defined as $\phi_{\text{trans}} = 0$) and where the torsion parameters are given by $C_1 = 1204.654$, $C_2 = 1947.740$, $C_3 = -357.845$, $C_4 = -1944.666$, $C_5 = 715.690$, and $C_6 = -1565.572$ with C_n/k_B in K. The external energy U^{ext} consists of a guest−guest intermolecular energy, a guest−zeolite interaction, and an intramolecular Lennard-Jones interaction

$$U^{\text{ext}} = U_{ij}^{\text{gg}} + U_{ij}^{\text{gz}} + U_{ij}^{\text{intra}} \tag{5}$$

with

$$U_{ij}^{\text{gg,gz,intra}} = \sum_{\text{LJ-pairs}} 4\epsilon_{ij}\left[\left(\frac{\sigma_{ij}}{r_{ij}}\right)^{12} - \left(\frac{\sigma_{ij}}{r_{ij}}\right)^{6}\right] - E_{\text{cut}} \tag{6}$$

where r_{ij} is the distance between site *i* and site *j*, $r_{\text{cut}} = 13.8$ Å is the cutoff radius, and E_{cut} is the energy at the cutoff radius. Jorgensen mixing rules, $\sigma_{ij} = \sqrt{\sigma_i \sigma_j}$ and $\epsilon_{ij} = \sqrt{\epsilon_i \epsilon_j}$, are used for the cross terms of the Lennard-Jones parameters, $\sigma = 3.75$ Å, $\epsilon/k_B = 98.0$ K for CH_3 and $\sigma = 3.95$ Å, $\epsilon/k_B = 46.0$ K for CH_2. The interactions between the zeolite and the guest molecules are assumed to be dominated by the oxygens atoms.[19] The interactions with the Si atoms are implicitly taken into account in this effective potential. The dispersive interactions with the oxygens are described with the Lennard-Jones potential with parameters $\sigma = 3.6$ Å and $\epsilon/k_B = 80$ K for O−CH_2 and $\epsilon/k_B = 58$ K for O−CH_3. Further details are given by Vlugt et al.[20] and Maesen et al.,[21] who have shown that with these parameters one can reproduce the adsorption isotherms, heats of adsorption, and Henry coefficients of various linear and branched alkanes in several zeolites accurately.

Instead of the experimentally studied cation-exchanged aluminosilicates, we use OFF-, ERI-, CHA-, and LTA-type silica devoid of cations. In all-silica sieves, the electric field does not vary much across the channels and cages and Coulomb forces can be neglected. The positions of the atoms are taken from ref 22. The zeolite is considered to be rigid[19] because this allows for the use of efficient grid interpolation techniques to compute interactions and forces. In cation-free all-silica sieves, there is evidence that adsorption and diffusivities are virtually unchanged for small alkanes when lattice vibrations are included.[23−25] Although with a fixed framework a flexible molecule cannot dissipate its energy, there is still some thermalization through the transfer of translational energy into the internal degrees of freedom of the molecule.

Conventional Monte Carlo (MC) is time-consuming for long chain molecules. The fraction of successful insertions into the sieve is too low. To increase the number of successfully inserted molecules, we apply the CBMC technique.[26,27] In the CBMC technique, a molecule is grown segment-by-segment. For each segment, we generate a set of *k* trial orientations according to the internal energy U^{int} and compute the external energy $U_i^{\text{ext}}(j)$ of each trial position *j* of segment *i*. We select one of these trial positions with a probability

$$P_i(j) = \frac{e^{-\beta U_i^{\text{ext}}(j)}}{\sum_{l=1}^{k} e^{-\beta U_i^{\text{ext}}(l)}} = \frac{e^{-\beta U_i^{\text{ext}}(j)}}{w(i)} \tag{7}$$

where $\beta = 1/(k_B T)$, k_B being the Boltzmann constant and *T* the temperature. The selected trial orientation is added to the chain and the procedure is repeated until the entire molecule has been grown. For this newly grown molecule, we compute the so-

called Rosenbluth factor[28]

$$W = \prod_i w(i) \tag{8}$$

The Rosenbluth factor of the new configuration is related to the free energy, F

$$\beta F = -\ln \frac{\langle W \rangle}{\langle W^{\mathrm{id}} \rangle} \tag{9}$$

where $\langle W^{\mathrm{id}} \rangle$ is the Rosenbluth factor of an ideal chain (defined as a chain having only internal interactions), which can be calculated from a simulation of a single chain. In addition, the Rosenbluth factor is related to the Henry coefficient, K_{H},

$$K_{\mathrm{H}} = \beta \frac{\langle W \rangle}{\langle W^{\mathrm{id}} \rangle} \tag{10}$$

In the limit of zero coverage, the Henry coefficient is related to the heat of adsorption, Q_{st}, via a thermodynamic relation[27]

$$Q_{\mathrm{st}} = -\frac{\partial \ln(K_{\mathrm{H}})}{\partial \beta} \tag{11}$$

Although this formula can be used to check the consistency, in practice, it is more convenient to obtain the heat of adsorption in the infinite dilution limit from

$$Q_{\mathrm{st}} = \langle U_{\mathrm{gz}} \rangle - \langle U_{\mathrm{z}} \rangle - \langle U_{\mathrm{g}} \rangle - k_{\mathrm{B}}T \tag{12}$$

where $\langle U_{\mathrm{gz}} \rangle$ and $\langle U_{\mathrm{g}} \rangle$ are the ensemble average of the potential energy of the zeolite−guest system and the energy of an isolated ideal chain, respectively and where the average zeolite energy, $\langle U_{\mathrm{z}} \rangle$, is zero for a rigid zeolite. The CBMC algorithm greatly improves the conformational sampling of molecules and increases the efficiency of chain insertions, required for the calculation of the free energy and Henry coefficients, by many orders of magnitude.

III. Transition-State Theory

ERI-, CHA-, and LTA-type zeolites consist of cages separated by 0.4 nm wide windows. These windows form large free energy barriers to diffusion. If the barrier is much higher than $k_{\mathrm{B}}T$, diffusion is an activated process. Once in a while a particle hops from one cage to the next, but the actual crossing time is negligible compared to the time a particle spends inside the cage. To compute the hopping rate from one cage to the next, the rare-event simulation techniques of Bennet and Chandler[14,15] can be readily applied. We give a brief overview of the main results of the Bennet−Chandler approach.

We consider a system that can be in two stable states, A and B. The reaction coordinate, a value that indicates the progress of the diffusion event from adsorption site A to site B, is denoted by q. Here, q is a function of the Cartesian coordinates, $\dot{q}$ denotes the derivative in time, q^* is the location of the dividing surface, and q_{A} and q_{B} are the minima of the free energy corresponding to states A and B, respectively. We introduce two characteristic functions, n_{A} and n_{B}, that measure whether the system is in state A or B. A possible and often used definition is

$$n_{\mathrm{A}} = \theta(q^* - q) \tag{13}$$

$$n_{\mathrm{B}} = \theta(q - q^*) \tag{14}$$

where θ is the Heaviside function $\theta(x)$, which has value zero for $x < 0$ and value 1 for $x \geq 0$. With these definitions, the transition rate, $k_{\mathrm{A}\to\mathrm{B}}$, is given by[16]

$$k_{A\to B} = \underbrace{\frac{\langle \delta(q^* - q) \rangle}{\langle \theta(q^* - q) \rangle}}_{P(q)} \times \underbrace{\frac{\langle \dot{q}(0)\delta(q^* - q)\,\theta(q(t) - q^*) \rangle}{\langle \delta(q^* - q) \rangle}}_{R(t)} \tag{15}$$

where $P(q)$ is the equilibrium probability density of finding the system at the top of the barrier divided by the equilibrium probability of finding it at state A and where $R(t)$ is the averaged flux at the top of the barrier multiplied by the probability that the system ends up in state B at time t. The expression is rigorously correct for arbitrary crossings provided that the barrier is much larger than $k_{\mathrm{B}}T$. $P(q)$ is a *time-independent* equilibrium quantity and can be computed explicitly

$$P(q) = \frac{\langle \delta(q^* - q) \rangle}{\langle \theta(q^* - q) \rangle} = \frac{\mathrm{e}^{-\beta F(q^*)}}{\int_{-\infty}^{q^*} \mathrm{e}^{-\beta F(q)}\,\mathrm{d}q} \tag{16}$$

where $F(q)$ is the free energy as a function of the diffusion path q. $R(t)$ is a conditional average, namely, the product $\dot{q}(0)\theta(q(t) - q^*)$, given that $q(0) = q^*$.

Using the assumption that the velocities of the atoms within the molecules follow a Maxwell−Boltzmann distribution, we can estimate from kinetic theory the long time value of $R(t)$ by $^1/_2|\dot{q}| = \sqrt{k_{\mathrm{B}}T/(2\pi m)}$, where m is the mass of the segments of the particle involved in the reaction coordinate (the total mass of the particle if the center of mass is used or the mass of only one segment if the reaction coordinate is a single segment like the middle bead in a molecule). Transition-state theory (TST) predicts a crossing rate $k_{\mathrm{A}\to\mathrm{B}}^{\mathrm{TST}}$ given by

$$k_{\mathrm{A}\to\mathrm{B}}^{\mathrm{TST}} = \sqrt{\frac{k_{\mathrm{B}}T}{2\pi m}} \frac{\mathrm{e}^{-\beta F(q^*)}}{\int_{-\infty}^{q^*} \mathrm{e}^{-\beta F(q)}\,\mathrm{d}q} \tag{17}$$

Calculating TST rate constants is therefore equivalent to calculating free energy differences. In the Bennet−Chandler approach, it is sufficient to assign the barrier position q^* inside the barrier region. The result of the scheme does not depend on the specific location, although the statistical accuracy does. If the dividing surface is not at the top of the barrier, the probability of finding a particle will be higher than that at q^*, but the fraction of the particles that actually cross the barrier will be less than predicted by transition-state theory. It is convenient to introduce the time-dependent transmission coefficient, $\kappa(t)$, defined as the ratio

$$\kappa(t) \equiv \frac{k_{\mathrm{A}\to\mathrm{B}}(t)}{k_{\mathrm{A}\to\mathrm{B}}^{\mathrm{TST}}} = \frac{\langle \dot{q}(0)\delta(q(0) - q^*)\theta(q(t) - q^*) \rangle}{\left\langle \left|\frac{1}{2}\right| \dot{q}(0) \right| \right\rangle} \tag{18}$$

The correction $\kappa(t)$ is the fraction of particles coming from the initial state that successfully reaches the final state out of those that cross the dividing surface at $t = 0$. It corrects for trajectories that cross the transition state from A but fail to equilibrate in B. It can be shown that $\kappa(0) = 1$ and $k_{\mathrm{A}\to\mathrm{B}}(0) = k_{\mathrm{A}\to\mathrm{B}}^{\mathrm{TST}}$. There is a large separation of time scales. The recrossings are completed in a time much less than the time to react, and eq 18 will reach a plateau value κ. For classical systems, $0 < \kappa \leq 1$, and eq 17 is corrected as

$$k_{\mathrm{A}\to\mathrm{B}} = \kappa k_{\mathrm{A}\to\mathrm{B}}^{\mathrm{TST}} \tag{19}$$

Standard molecular dynamics (MD) yields the transmission coefficients; a separate MC simulation yields the starting configurations. The reaction coordinate is restricted to the dividing surface q^*. The MC moves involved are translations of the reaction bead in the plane of the dividing surface and complete regrowing of the molecule starting from the restricted bead. Subsequently the transmission coefficient is calculated by standard MD in the microcanonical ensemble using a velocity Verlet integrator with a time step of 0.2 fs. The beads are given independent velocities, corresponding on average to the desired temperature, by sampling from a Maxwell−Boltzmann distribution. A molecule sampled at a particular temperature at the top of the barrier will acquire a huge velocity once it has arrived in the valley. No thermal equilibration takes place. In fact, the velocity is so high that it will very likely cross another window or (as in ERI- and CHA-type structures) bounce back from the opposite wall and recross the initial window again. For this reason, it is necessary to terminate a trajectory once a valley has been reached. Failing to end the trajectory can lead to spurious, undamped oscillations in $\kappa(t)$.

The approach of $\kappa(t)$ to its plateau value can be quite slow.[16] Moreover, in the case of diffusive barrier crossings the transmission coefficient is quite small and κ *cannot* be calculated accurately by using eq 15. The Bennet−Chandler approach becomes inefficient for systems with low transmission coefficients because the scheme prepares the system in a state that is not close to the steady-state situation. In addition, the scheme employs the θ-function to detect what state the system is in. The scheme can be improved by devising a perturbation that prepares the system immediately close to the steady state and by constructing a more continuous detection function.

One of the problems when devising a more sophisticated scheme is the lack of exact knowledge of the free energy of the system as a function of the order parameter. It is shown that in practice we need to approximate only $F(q)$.[16] We denote our estimate of $F(q)$ by $F_{\text{est}}(q)$. Any reasonable guess will lead to a more rapid convergence than the δ function. Using the free energy estimate, we can compensate approximately for the effect of the energy barrier. This leads to a more or less uniform distribution over the entire range of q. Only trajectories starting in the barrier region yield relevant information, and therefore, a weighting function, $w(q)$, is applied, restricting the sampling to the barrier region:

$$w(q) = \frac{e^{2\beta F_{\text{est}}(q)}}{\int_{q_A}^{q_B} e^{2\beta F_{\text{est}}(q)}\, dq} \tag{20}$$

The following expression for $k_{A\to B}$ can be derived:[16]

$$k_{A\to B} = \frac{\int_{q_A}^{q_B} e^{2\beta F_{\text{est}}}\, dq}{[\int_{q_A}^{q_B} e^{\beta F_{\text{est}}}\, dq]^2} \frac{\langle w(q)\rangle_{\text{eq}}}{\langle n_A\rangle_{\text{eq}}} \times \int_0^\infty \langle \dot{q}(0)\dot{q}(t)\, e^{\beta F_{\text{est}}(q(t))-\beta F_{\text{est}}(q(0))}\rangle_w\, dt \tag{21}$$

If $F(q)$ is known in advance or, as in our case, $F_{\text{est}}(q)$ is the best possible measurement in a simulation, then $F_{\text{est}}(q)$ and $F(q)$ become synonymous. This leads to a simplification of the expressions

$$\kappa(t) = \frac{e^{\beta F(q^*)}}{\int_{q_A}^{q_B} e^{\beta F(q)}\, dq} \frac{2}{\langle|\dot{q}|\rangle} \int_0^\infty \langle \dot{q}(0)\dot{q}(t)\, e^{\beta F(q(t))-\beta F(q(0))}\rangle_w\, dt \tag{22}$$

$$k_{A\to B} = \frac{\int_0^\infty \langle \dot{q}(0)\dot{q}(t)\, e^{\beta F(q(t))-\beta F(q(0))}\rangle_w\, dt}{\int_{q_A}^{q_B} e^{\beta F(q)}\, dq \int_{-\infty}^{q^*} e^{-\beta F(q)}\, dq} \tag{23}$$

At infinite dilution, the molecules perform a random walk on a lattice spanned by the cage centers. The transmission rates are easily converted to diffusion coefficients if the jump distance and the number of equivalent diffusion paths are known.[29] Error calculations are performed for the measured quantities, including the free energy profiles $F(q)$, the heats of adsorption, the Henry coefficients, and the diffusion coefficients. Each insertion of a chain molecule is statistically independent, and error bars are easily calculated for each point on the free energy profile and for the Henry coefficients. Error bars on the diffusion coefficients, obtained from the transmission rate k_{AB}, are less trivial. The complete free energy profile is regenerated for each point from their average value and error value σ, assuming a Gaussian distribution with width σ around its average value.[30] A smooth cubic approximation spline is fitted to the regenerated data, and eq 16 is evaluated using the spline approximation. The procedure is repeated many times, and the error $P(q)$ is assumed to be twice the standard deviation in the resulting dataset (95% confidence interval). The error in the diffusion coefficient is then calculated by applying normal error propagation rules.

IV. Reaction Coordinate

To compute the free energy as a function of the position in the zeolite, one has to relate a position in the channel or cage to a reaction coordinate q. Such a map should satisfy several criteria: (i) Every coordinate in the simulated volume should uniquely designate a position in a single cage. (ii) All Cartesian space should be used and partitioned into equivalent regions to have a correct entropic contribution. Not only all pore volume but also the zeolite volume should be used. The space group of the zeolite indicates how to exploit the inherent symmetry. (iii) The mapping should achieve the highest free energy barrier. If not, the transmission coefficient can become very small, making the computation extremely inefficient or even impossible. In addition, a linear mapping is preferred from a computational point of view to avoid correcting the density distribution for the use of constraints.[16]

We stress that choosing an appropriate reaction coordinate is vital. By trial and error, we concluded that using the second bead of the alkane chain gave near optimal results for all alkane chains and zeolites discussed here. Chains are always newly grown starting from this bead. The mapping is depicted in Figure 1, where a part of the ERI-type silica is shown with cages A and B (connected to other cages) sliced half open. Two examples of the mapping are depicted: a C_{14} chain in cage A and a C_{10} chain in cage B. Free energy values are mapped onto the one-dimensional free energy profile $F(q)$ by orthogonal projection of the position of the second bead onto the line perpendicular to the window. Only chains that have the smallest distance to either cage A or cage B (of all of the cages in the zeolite) give a contribution to the transmission rate $k_{A\to B}$.

There are two ways to obtain a near-optimal mapping: try all beads, compute the free energy profiles, and then choose the one that gives the highest free energy difference, or try all beads, compute the transmission coefficient κ, and then choose the one that gives the highest κ. Figure 2 shows the free energy profiles (raw, unsmoothed data) in ERI-type silica at 600 K for mappings using the various beads of C_9 as the order parameter. The maximum of the free energy is at the $q = 0$ position

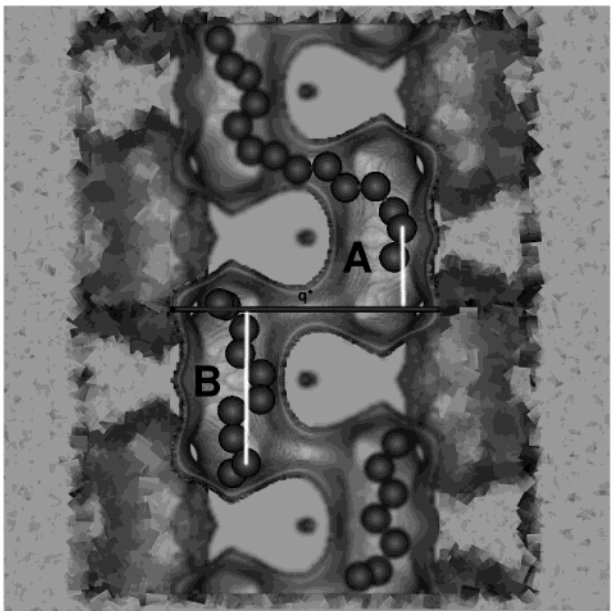

Figure 1. The reaction coordinate q, indicating the progress of the diffusion event from adsorption site A to adsorption site B, is defined as the position of the second bead of a chain mapped orthogonal to the axis of projection (the line perpendicular to the window). The resulting free energy profile $F(q)$ indicates a high free energy barrier at the position of the window q^* separating cage A and B. Shown here are two examples in ERI-type silica: C_{14} in cage A and C_{10} in cage B. Also shown is a C_8 molecule, but it would contribute to the diffusion between cage B and the C_8 cage (these contributions can be converted into a $k_{A\rightarrow B}$ contribution due to symmetry reasons). The C_8 molecules fit snugly inside the erionite cages, C_{10} adapts high-energy configurations, while the C_{14} stretches energetically more favorably across two cages.

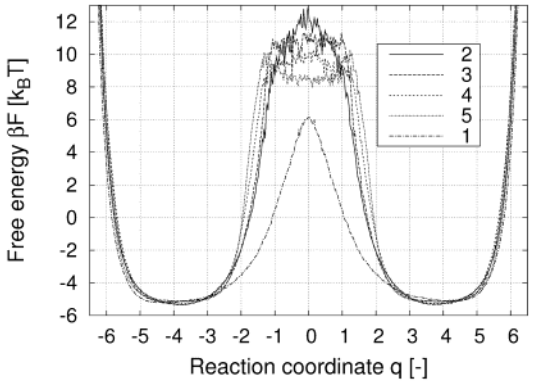

Figure 2. Free energy profiles $F(q)$ (raw, unsmoothed data) in ERI-type silica at 600 K for C_9 using bead 1, 2, 3, 4, and 5 as the mapping bead (lines from top to bottom at $q = 0$ in order of the legend).

corresponding to the dividing window q^*; the minimum values are at $q \approx |4|$ corresponding to values deep inside cages A and B. We note that the x-axis corresponds to the line perpendicular to the window in Figure 1. The second-bead mapping gives the highest free energy barrier, and in addition, the shape of the free energy profile indicates that molecules will fall off the barrier most rapidly. With the second bead on top of the barrier, the tail of the chain is bent and close to the wall. It has already one bead through the window, and combined with the asymmetry of the molecule, it is dynamically most balanced. With use of the middle-bead mapping (bead 5), it is nearly impossible to obtain κ. The chain tends to sit comfortably in a (small) local free energy minimum and diffuses on top of the barrier without actually falling off the barrier. For other chain lengths, similar results have been obtained.

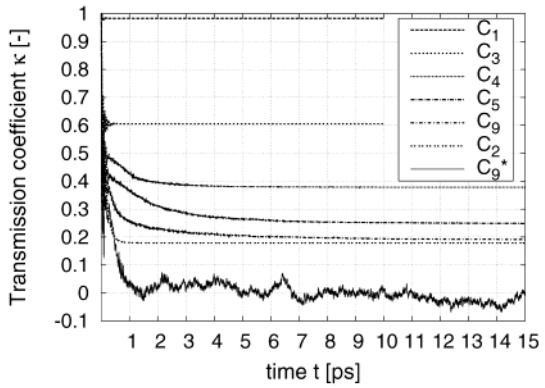

Figure 3. Transmission coefficients $\kappa(t)$ in ERI-type silica at 600 K plotted against simulation time for C_1-C_5 and C_9 using the second-bead mapping and C_9^* using the middle -bead mapping (lines from top to bottom in order of the legend).

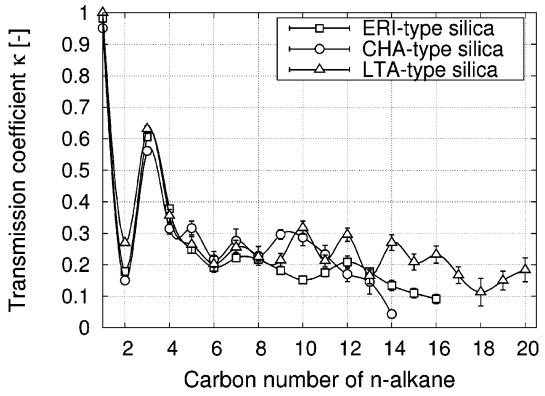

Figure 4. Transmission coefficients in ERI-, CHA-, and LTA-type silica plotted as function of carbon number of the *n*-alkane. Error bars are only shown when larger than the symbol size.

In Figure 3, we show the transmission coefficient $\kappa(t)$ for C_1-C_5 and C_9 for ERI-type silica at 600 K with a second-bead mapping. For comparison, we show the result for C_9 with a middle-bead mapping. The position of the middle bead cannot be used because $\kappa(t)$ does not reach a clear positive plateau value. Note that a change in the barrier height results in an exponential change of the transmission coefficient. Computing the transmission coefficient for the various mappings is therefore more sensitive. Figure 4 shows the transmission coefficient κ as a function of chain length at 600 K for the zeolites ERI-, CHA-, and LTA-type silica. The second-bead mapping works well, and the transmission coefficients are for chain lengths of C_3 or greater of approximately equal magnitude ($\kappa = 0.1-0.3$). This facilitates the interpretation and comparison of the free energy profiles as a function of chain length.

The free energy profiles (in combination with the transmission coefficients) can be used to calculate $k_{A\rightarrow B}$. The Ruiz-Montero et al. method uses the free energy profile to define a weighting function, $w(q)$, for sampling initial configurations. In Figure 5, we show the histogram of the position of the second bead of propane chains around q^* in ERI-type silica. The shape of the distribution is proportional to $e^{\beta F_{est}(q)}$ with $F_{est}(q)$ being the free energy profile of propane. The sampled configurations are then used to measure the diffusion coefficient on top of the barrier by calculating the velocity autocorrelation function taking the weighting function into account. In Table 1, we compare the

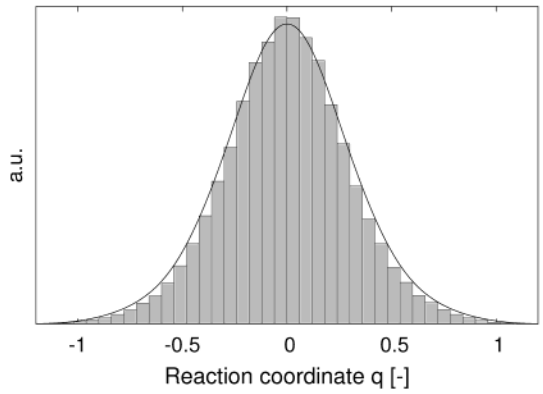

Figure 5. Histogram of the sampled positions of the second bead of propane in ERI-type silica. The $q = 0$ position corresponds to the position of the dividing window. The solid curve denotes the curve $e^{\beta F(q)}$, $F(q)$ being the spline fit through the free energy profile of propane.

diffusion results for both methods for C_1-C_9 in ERI-type silica at 600 K. The Bennet−Chandler method is performed using the second-bead mapping, while the Ruiz-Montero et al. method is performed with the middle-bead mapping. Note that the methods are equal for C_1-C_4. The results are consistent, and although the statistics is rather poor, the Ruiz-Montero et al. method worked for this poor choice of reaction coordinate where the Bennet−Chandler method completely failed. It provides much more freedom and worked for several mappings, including the ones that have inherent diffusive behavior on top of the barrier. The validity of the diffusion results was checked by using both methods.

V. Zeolite Description

Small differences in the crystal structure of silica cause large differences in the diffusion rates of an alkane as a function of chain length. The OFF-type silica structure[31] crystallizes in the hexagonal-ditrigonal dipyramidal space group $P\bar{6}m2$ with $a = 1.31$ nm, $b = 1.31$ nm, and $c = 0.76$ nm and $\alpha = \beta = 90°$ and $\gamma = 120°$. In the absence of stacking faults, OFF-type silica would consist of channels 0.67 nm across. The perpendicular 0.36−0.49 nm wide windows have a significantly slower diffusion rate and are only accessible to small molecules. The pores are girthed at 0.76 nm intervals by 12T-membered ring structures of approximately 0.67 nm × 0.68 nm. The ERI-type silica structure[32] crystallizes in the hexagonal dipyramidal space group $P6_3/mmc$ with $a = b = 1.31$ nm and $c = 1.52$ nm and $\alpha = \beta = 90°$ and $\gamma = 120°$. The elongated erionite cages are approximately the shape of 1.3 nm × 0.63 nm cylinders connected by 0.36 nm × 0.51 nm windows. Only linear molecules are able to penetrate the windows. There are three windows at the top of the cage rotated 120° with respect to each other. At the bottom of the cage, there are also three windows rotated 120° with respect to each other. The top three windows are aligned with the windows at the bottom. Zeolite T is an intergrowth of OFF- and ERI-type zeolites.[33] It consists primarily of OFF-type zeolite interspersed by thin layers of ERI-type zeolite. Each ERI-type cage blocks an OFF-type channel and forces diffusion through the ERI-type window. The CHA-type structure[34] has the spacegroup $R3m$ (a squashed cube) with $a = b = c = 0.942$ nm and $\alpha = \beta = \gamma = 94.47°$. The CHA-type cage is an ellipsoidal cavity of about 1.0 nm × 0.67 nm across, accessible through 0.38 nm wide windows. Only linear alkanes are able to penetrate the windows. There are three windows at the top of the cage rotated 120° with respect to each other. At the bottom of the cage, there are also three windows rotated 120° with respect to each other. The bottom three are at a 120° angle relative to the top ones. The LTA-type structure[35] has a cubic spacegroup $Fm\bar{3}c$ with $a = b = c = 2.4555$ nm and $\alpha = \beta = \gamma = 90°$. The crystallographic unit cell consists of 8 large spherical cages (named α-cages) of approximately 1.12 nm interconnected via windows of about 0.41 nm diameter.

In Figure 6a−d, we show the volume-rendered pictures of the OFF-, ERI-, CHA-, and LTA-type silica, respectively. The unit cell is divided into 150 × 150 × 150 voxels (constant valued volume elements). At millions of random positions in the unit cell, the free energy of a test particle (methane molecule) is calculated and assigned to the appropriate voxel. To visualize this energy landscape, the three-dimensional dataset is volume-rendered,[36,37] removing the parts that generate overlap (the zeolite itself) by making it completely transparent. Low-energy values are rendered with medium transparency, allowing the inside of the cages to be viewed as voids. Higher energy values are rendered less and less transparent until the energy approaches a cutoff energy and is regarded as part of the zeolite wall. For simulation efficiency, all structures are converted to orthorhombic periodic unit cells with dimensions $a = 2.3021$ nm, $b = 1.3291$ nm, and $c = 0.7582$ nm for OFF, $a = 2.2953$ nm, $b = 1.3252$ nm, and $c = 1.481$ nm for ERI, and $a = 1.5075$ nm, $b = 2.3907$ nm, and $c = 1.3803$ nm for CHA. In addition to the relevant cages and channels, there are also topologically disconnected pockets. A methane molecule does fit at that position, but it is not accessible from the main cages and channels. An example is the visibly disconnected SOD-type sodalite cage (β-cage) in LTA. To obtain correct results, it is necessary to artificially block the inaccessible pockets for adsorbing molecules.

TABLE 1: Comparison of Two Transition-State Theory Methods for Computing Diffusion Constants in the Zeolite Erionite for C_1-C_9[a]

n	D^{TST} [m^2/s]	κ	D_{BC} [m^2/s]	D_{RM} [m^2/s]
1	$1.31 \times 10^{-12} \pm 1.33 \times 10^{-14}$	0.983 ± 0.002	$1.3 \times 10^{-12} \pm 1.3 \times 10^{-14}$	$1.3 \times 10^{-12} \pm 2.4 \times 10^{-14}$
2	$1.85 \times 10^{-13} \pm 3.06 \times 10^{-15}$	0.179 ± 0.002	$3.3 \times 10^{-14} \pm 6.5 \times 10^{-16}$	$4.4 \times 10^{-14} \pm 2.0 \times 10^{-14}$
3	$1.71 \times 10^{-16} \pm 1.92 \times 10^{-17}$	0.606 ± 0.003	$1.0 \times 10^{-16} \pm 1.2 \times 10^{-17}$	$1.0 \times 10^{-16} \pm 8.5 \times 10^{-18}$
4	$7.46 \times 10^{-16} \pm 1.03 \times 10^{-16}$	0.378 ± 0.007	$2.8 \times 10^{-16} \pm 3.9 \times 10^{-17}$	$2.8 \times 10^{-16} \pm 2.6 \times 10^{-17}$
5	$1.48 \times 10^{-15} \pm 2.59 \times 10^{-16}$	0.249 ± 0.009	$3.7 \times 10^{-16} \pm 6.6 \times 10^{-17}$	$4.3 \times 10^{-16} \pm 5.0 \times 10^{-17}$
6	$3.86 \times 10^{-15} \pm 8.14 \times 10^{-16}$	0.192 ± 0.009	$7.4 \times 10^{-16} \pm 1.6 \times 10^{-16}$	$5.1 \times 10^{-16} \pm 9.4 \times 10^{-17}$
7	$1.53 \times 10^{-15} \pm 3.94 \times 10^{-16}$	0.222 ± 0.012	$3.4 \times 10^{-16} \pm 8.9 \times 10^{-17}$	$2.6 \times 10^{-16} \pm 2.2 \times 10^{-16}$
8	$8.95 \times 10^{-16} \pm 3.00 \times 10^{-16}$	0.217 ± 0.012	$1.9 \times 10^{-16} \pm 6.6 \times 10^{-17}$	$4.6 \times 10^{-16} \pm 4.4 \times 10^{-16}$
9	$2.93 \times 10^{-15} \pm 1.25 \times 10^{-15}$	0.182 ± 0.011	$5.3 \times 10^{-16} \pm 2.3 \times 10^{-16}$	$4.1 \times 10^{-16} \pm 3.8 \times 10^{-16}$

[a] The Bennet-Chandler method uses the second-bead mapping and dynamically corrects the transition-state estimate, k^{TST}, with the transmission coefficient, κ. The diffusion coefficient, D_{BC}, is computed as κD^{TST}. The diffusion coefficients D_{RM} in the last column are obtained using the Ruiz-Montero et al. method. Here, the mapping used was the middle-bead mapping, which did not work for the second-bead mapping because of the extremely low transmission coefficients.

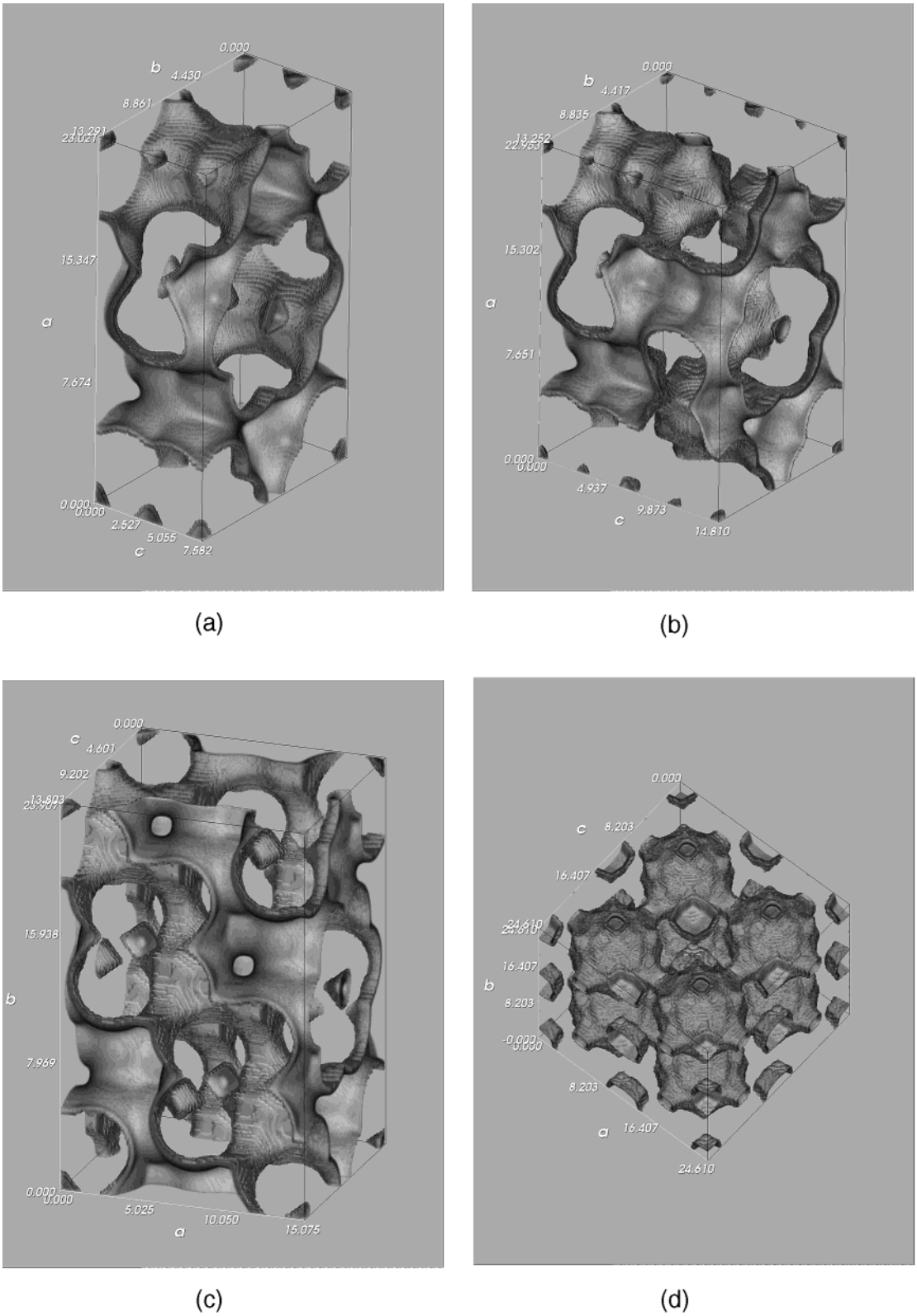

Figure 6. The structure of a single periodic unit cell of (a) OFF-type silica, (b) ERI-type silica, (c) CHA-type silica, and (d) LTA-type silica. Distance labels are plotted in units of Å.

To examine the critical molecular length at which molecules are forced to stretch into two cages, the silica structures are probed with molecules of various lengths. The simulation snapshots are visually inspected and end-to-end distance histograms (data not shown) are studied. The OFF-type channels can host all chain lengths. The largest molecule that fits in a single ERI-type cage is *n*-C_{13}. It assumes a serpentine-like configuration extending tethered between opposite windows, which makes it about 1.6 nm long. Similarly, 1.35 nm long *n*-C_{11} is the longest molecule that can be tethered between two opposing windows in a CHA-type cage. An LTA-type cage can harbor molecules as long as *n*-C_{22}−*n*-C_{24} in a conformation coiled like a snake in a basket. Pictures of these snapshots are published in ref 6.

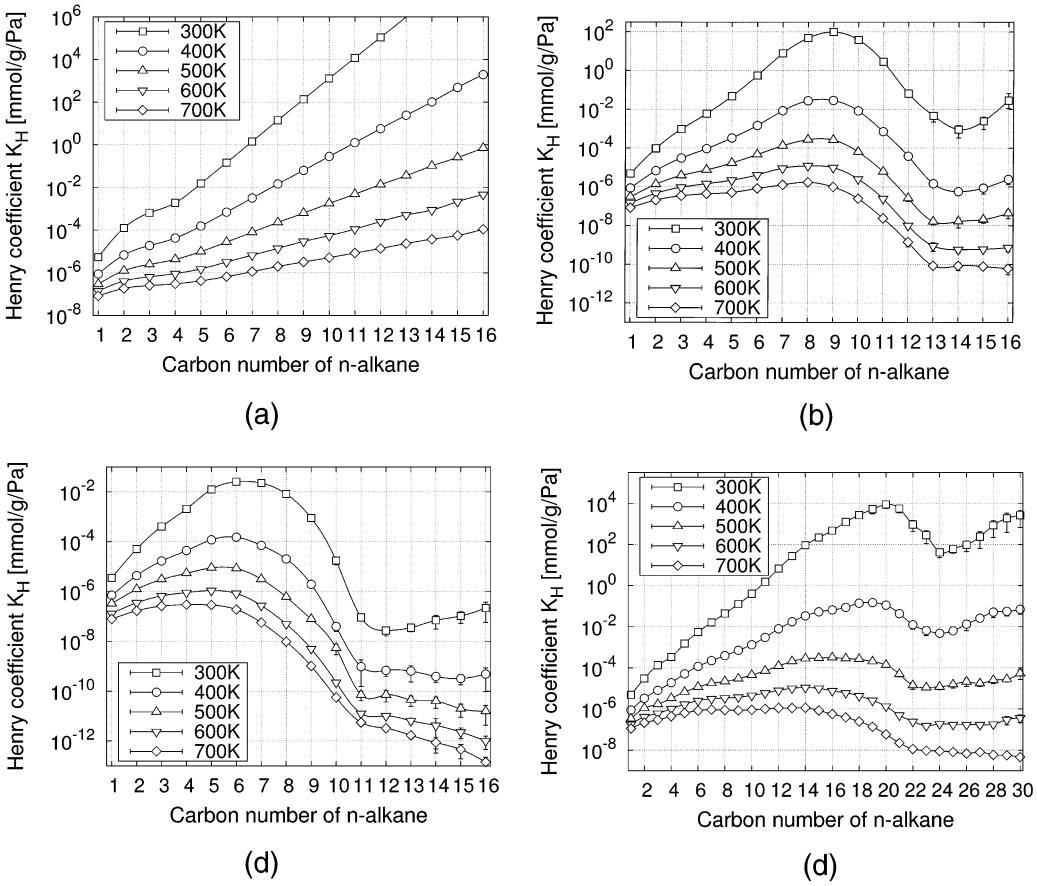

Figure 7. Henry coefficients as a function of chain length at various temperatures for (a) OFF-type silica, (b) ERI-type silica, (c) CHA-type silica, and (d) LTA-type silica. At low pressure, the loading is linear in the pressure with the Henry coefficient as the proportionality constant. Error bars are only shown when larger than the symbol size.

VI. Results and Discussion

A. Henry Coefficients and Isosteric Heats of Adsorption. Molecular sieves have the ability to trap molecules that can access their intracrystalline void volume. For low pressures, the amount of adsorbed molecules is linearly related to the pressure, the Henry coefficient being the proportionality constant. If the external pressures are sufficiently low, the Henry coefficient provides a good estimation of the extent of adsorption isotherms. In Figure 7a, the Henry coefficients at various temperatures as a function of chain length for OFF-type silica are shown. The Henry coefficients increases exponentially with alkane chain length because the enthalpy gained by molecule−wall interaction outweighs the loss in entropy. Other channel structures such as MFI- and TON-type silica exhibit a similar pattern.

ERI- and CHA-type zeolites show a markedly different behavior (Figure 7b,c). A clear cage effect of many orders of magnitude is present: a periodic, nonmonotonic dependence of the Henry coefficient on chain length. The local maximum indicates that the shape of *n*-C_8−*n*-C_9 is commensurate with the shape of an ERI-type cage, whereas the shape of *n*-C_5−*n*-C_6 is commensurate with that of a CHA-type cage. A sharp decrease in the Henry coefficient is observed when molecules are forced to curl up so as to fit into a single cage. When they are even longer, this conformation becomes too unfavorable, and they stretch across two cages instead. In ERI-type silica, the first molecule to stretch across two cages is *n*-C_{14}; in CHA-type silica, it is *n*-C_{12}. This neatly reflects the difference in size between the ERI- and CHA-type cages. Increasing the chain length improves adsorption again, until the molecule has to curl up and eventually has to stretch across three cages. As opposed to the small, elongated ERI- and CHA-type cages, molecules have more orientational freedom in the spherical, larger LTA-type cages. As a result, the length of *n*-alkane that fits best is more temperature-dependent than those for ERI- and CHA-type silica. At 300 K, the molecule that fit most snugly is *n*-C_{20}; at 500 K, it is *n*-C_{14}−*n*-C_{18}, while at 700 K, the plateau stretches from *n*-C_6 to *n*-C_{14}. The largest molecules that fit inside a single cage are C_{22}−C_{24} and represent the local minimum in the Henry coefficient.

For all silicas studied here, the adsorption decreases with increasing temperature because the thermal energy increase causes a lowering of the physisorption energy. The positions of the maxima, that is, the best adsorbing molecules, shift toward lower chain lengths for increasing temperature. The maxima themselves become broadened and can even become large plateaus of equally well adsorbing molecules. Also the local minima shift toward lower chain lengths with increasing temperatures. The position of these minima indicates a crossover point. Below this crossover point, the molecules fit into a single cage; above this point, the chains start to find it energetically more favorable to stretch across two cages.

The heat of adsorption, Q_{st}, is related to the Henry coefficient. The isosteric heat of adsorption obtained from simulation is plotted in Figure 8 as a function of chain length for OFF-, ERI-, CHA-, and LTA-type silica. The heat of adsorption is obtained from a single *NVT* (600 K) simulation in the gas phase and a single simulation of one molecule adsorbed in ERI-type silica, measuring the average energies as needed in eq 12. The result is consistent with the thermodynamic limit, eq 11, where we obtained the heat of adsorption as an average over a temperature

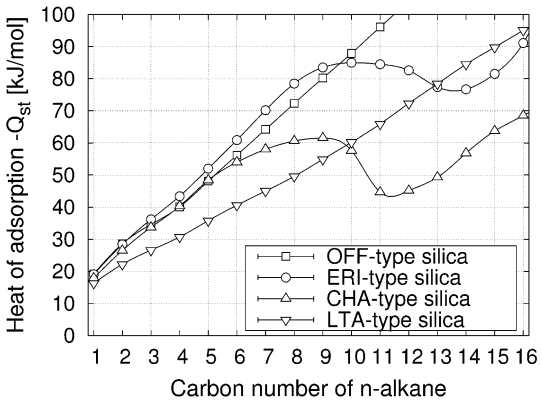

Figure 8. Heat of adsorption, $-Q_{st}$, as a function of chain length of the alkanes adsorbed in OFF-, ERI-, CHA-, and LTA-type silica at 600 K using eq 12. Error bars are only shown when larger than the symbol size.

range. The heat of adsorption has only a slight temperature dependence for these silicas. We were unable to find comparative experimental data on ERI-, CHA-, or LTA-type silica or aluminum phosphates. The heat of adsorption for OFF-type silica is directly proportional to the alkane length, while that of ERI- and CHA-type silica shows a nonmonotonic, periodic behavior with similar periods as those of the Henry coefficient data. The heat of adsorption, Q_{st}, in LTA-type silica is also nonmonotonic, although only for alkanes longer than C_{21} (data not shown).

Many zeolites show a well-defined linear variation of adsorption energy with carbon number and a linear relationship between the entropy and energy of adsorption (compensation effect). In ref 38, Ruthven and Kaul present such correlations for sorption of linear alkanes on the Na form of zeolite X, the Na form of zeolite Y, ultrastable zeolite Y, and silicalite. We found that pores with constrictions (*windows*) that approach the diameter of the adsorbate exhibit a dramatically different behavior. Instead of attractive adsorbate−adsorbent interactions, windows exert repulsive adsorbate−adsorbent interactions that increase the adsorption enthalpy of any *n*-alkane partially adsorbed inside such a window. Accordingly, the usual compensation between adsorption enthalpy and adsorption entropy ceases as soon as *n*-alkanes become too long to fit comfortably inside the wider part of these pores (*cages*).[6] Our simulations indicate that the compensation theory is true for channel-type zeolites but for cage/window-type zeolites with windows smaller than approximately 0.45 nm the results apply only to effective chain lengths much smaller than the cage size. At higher carbon numbers, the data deviate and the linear relationship breaks down.

B. Diffusion. The simulation results of diffusion of *n*-alkanes in ERI-type silica as a function of chain length at several fixed temperatures are presented in Figure 9a, while the experimental results found by Gorring on a potassium-exchanged intergrowth of OFF- and ERI-type zeolites are plotted in Figure 9b. The order of magnitude and overall trend is well reproduced. The simulation data clearly support the existence of a diffusional window effect. The positions of the minima at C_8 and the maxima at $C_{12}-C_{13}$ are well in agreement with Gorring's experimental data. In addition to the C_8 minimum, the simulation data shows a second local minimum at C_3.

In Figure 10a, we plot the simulation results for CHA-type silica, and the experimental curve of Gorring is shown in Figure 10b. Also the simulated data for CHA-type silica corroborate the existence of a diffusional window effect with the maximum diffusion rate at $C_{10}-C_{11}$. The overall shape of the diffusion curve is satisfactorily reproduced. The simulation data find the local minima at C_3, while the Gorring results indicate a C_5 minimum, although the difference is small.

The behavior found for ERI- and CHA-type silica is markedly different from that of LTA-type silica (Figure 11a). The experimental results taken from refs 39 and 40 are plotted in Figure 11b. The activation energies reported in the references are used to extrapolate the experimental diffusion coefficients to 600 K. In ref 39, the authors explicitly state that no evidence for a window effect in LTA-type zeolites has been found. Our simulation data agree qualitatively well with the experimental results, and also the order of magnitude is well reproduced for LTA-type silica. A possible window effect is, however, expected at higher chain lengths ($C_{23}-C_{24}$) than have been studied experimentally. In addition, our simulation data seem to suggest that the slight decrease in diffusion beyond the C_{10} region corresponds to the critical length at which molecules feel the limitation of the cage and start to fold or coil.

For all silicas studied here, the diffusion coefficient decreases with decreasing temperature. The positions of the maxima and minima shift toward lower chain lengths for decreasing temperature. The window effect in ERI- and CHA-type silica is several orders in magnitude and increases with lower temperatures. LTA-type silica does not possess an order of magnitude window effect in the C_1-C_{20} range but shows complex intracage

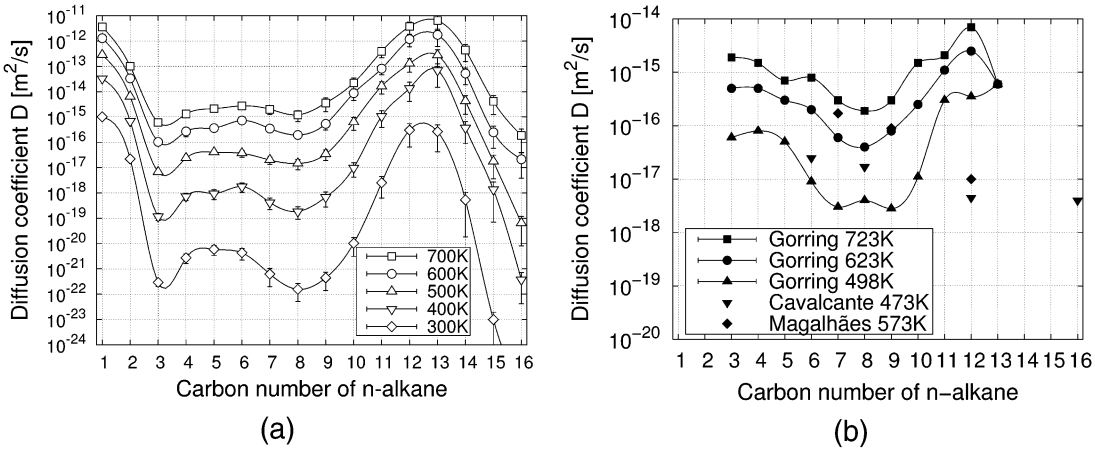

Figure 9. Diffusion coefficients as a function of chain length at various temperatures in ERI-type zeolite: (a) silica simulation results; (b) experimental results of Gorring on a potassium-exchanged OFF/ERI intergrowth,[2] Cavalcante et al.,[12] and Magalhães et al.[13] Error bars on the simulation data are only shown when larger than the symbol size.

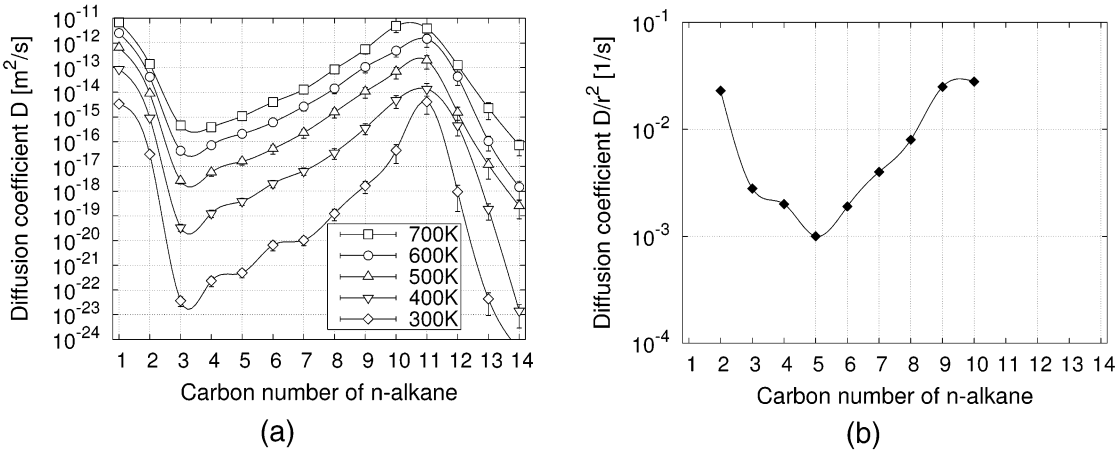

Figure 10. Diffusion coefficients as a function of chain length at various temperatures in CHA-type zeolite: (a) silica simulation results; (b) experimental results of Gorring on H−CHA[3] (the crystal size *r* is unknown). Error bars on the simulation data are only shown when larger than the symbol size.

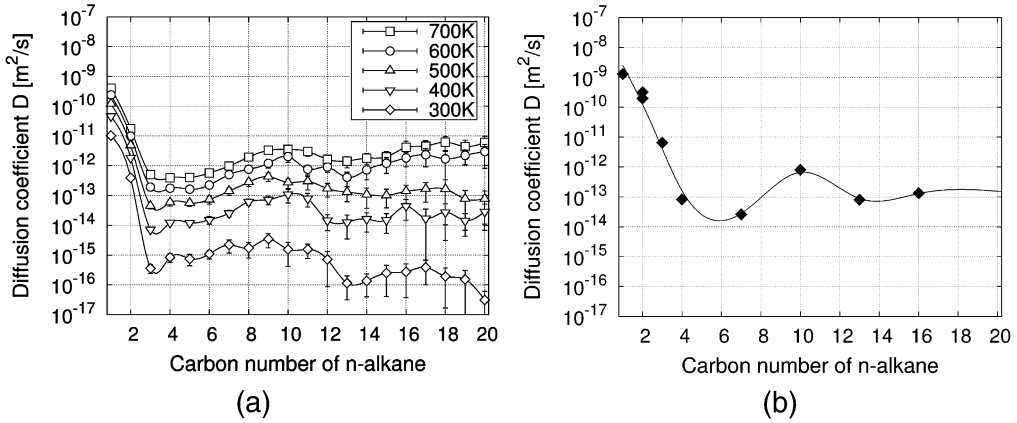

Figure 11. Diffusion coefficients as a function of chain length at various temperatures in LTA-type zeolite: (a) silica simulation results; (b) experimental results of Eic and Ruthven[39] on the Ca/Na form of LTA-type zeolite. Error bars on the simulation data are only shown when larger than the symbol size.

behavior. The agreement between simulated data on a cation-free LTA-type sieve and the experimental data on a cation-loaded LTA-type zeolite is remarkable.

Gorring provided an explanation for the window effect in terms of a match between the effective length of a molecule and the size of the zeolite cage (the window-to-window distance).[2] Eic and Ruthven applied similar logic to LTA-type zeolites.[39] They argued that the maximum activation energy should then occur at $C_{13}-C_{14}$ in the LTA-type structure. When they found that the activation energy increased monotonically with carbon until C_{16}, they dismissed the window effect. Our simulations indicate that they did not take adequately into effect that molecules usually curl and fold into energetically more favorable conformations and thereby reduce their effective length.[6] Simulations predict that a window effect for LTA-type silica will occur, not at the chain lengths predicted by Eic and Ruthven, but around chain length C_{24}.

We obtained convincing evidence of a diffusional window effect for both ERI- and CHA-type silica with positions for the maxima of diffusion corresponding to the cage size, as suggested by Gorring. The simulation results agree qualitatively with Gorring's experimental results but deviate somewhat for small chain lengths in ERI-type silica. Discrepancies are not surprising because we model Gorring's complicated intergrowth of ERI- and OFF-type zeolites loaded with potassium cations with ERI-type silica. Figure 12 depicts two OFF-type channels, one of which is blocked by an ERI-type intergrowth. ERI-type moieties

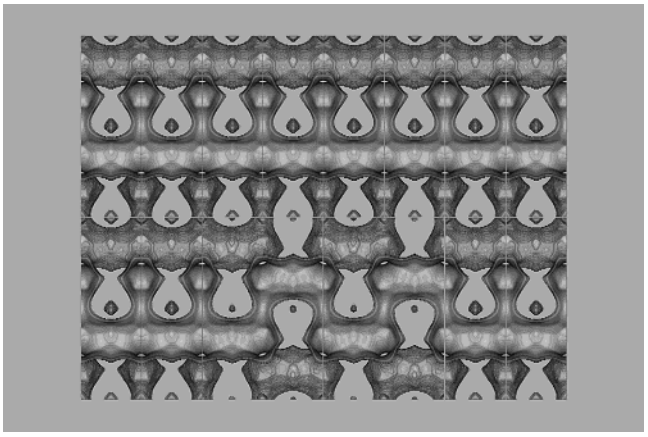

Figure 12. Zeolite T is a disordered intergrowth of OFF- and ERI-type zeolite and crystallographically not well defined. Although OFF-type zeolite is dominating, it is believed that ERI-type zeolite is the controlling bottleneck for diffusion. The top channel is an unobstructed offretite channel; the bottom channel is blocked by two unit cells ERI-type zeolite. The exact arrangement of the ERI-type intergrowth inside OFF-type zeolite is unknown, although ERI-type zeolite is thought to form thin layers converting OFF-type zeolite into a zeolite that can only adsorb linear molecules.

only block the OFF-type channels for molecules larger than C_4. A portion of the small molecules can easily "navigate" around the ERI-type block. They have so much orientational freedom

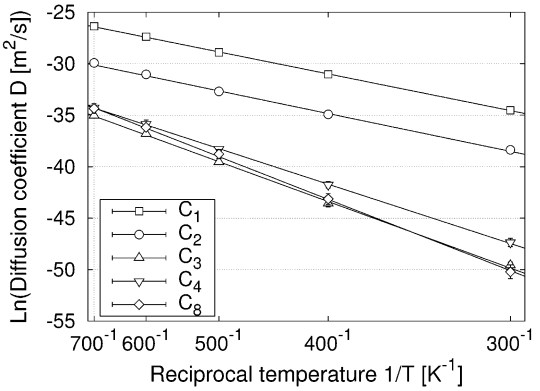

Figure 13. The natural logarithm of the diffusion coefficient in ERI-type silica plotted against the reciprocal temperature for C_1-C_4 and C_8. The data are fitted with a straight line over the complete simulated temperature range showing Arrhenius-type behavior of the form $D_\infty\, e^{-E_D/(k_BT)}$. Error bars are only shown when larger than the symbol size.

that the diffusion path into the OFF-type side cages is just as tortuous as the diffusion into the ERI-type moieties. These diffusional short cuts for *n*-C_4 chain length and lower could contribute to a change in diffusion rate by orders of magnitude.

C. Activation Energies and Frequency Factors. For the OFF/ERI intergrowth[2,12,13] and both the Ca/Na and Na forms of LTA-type zeolites,[39,40] experimental data on diffusion activation energies are available. There are also some data on frequency factors in the K form of the OFF/ERI intergrowth[2] and the Ca/Na form of the LTA-type zeolite.[39] In our simulations, we use all-silica with the equivalent framework structure but without nonframework cations. Accordingly, the simulation data show the influences of the structure of the zeolite itself and exclude loading and cation effects.

To calculate the activation energy and frequency factor in simulation, we exploit the fact that diffusion in cage zeolites can be described as an activated process. If the jump distance is l and we have n equivalent jump sites and d is the dimensionality, we can use the Einstein equation and relate the diffusion coefficient to the jump rate,

$$D(T) = \frac{nl^2\nu_0}{2d}\, e^{-(E_V+E_A/(k_BT))} = D_\infty\, e^{-(E_D/(k_BT))} \qquad (24)$$

Here, ν_0 can be though of as an attempt frequency (frequency of oscillation) at the free energy minima, E_A is the hopping activation energy, and E_V is the vacancy formation energy. At infinite dilution, the vacancy formation energy is zero. The self-diffusion activation energy, E_D, is the energy needed to "activate" the diffusion ($e^{-E_D/(k_BT)}$ being the probability that the molecule has enough energy). The preexponential factor or frequency factor, D_∞, is a material property of both the zeolite and the diffusing molecule. It accounts for directional steric effects that are difficult to predict.

Figure 13 plots the logarithm of the diffusion coefficient as a function of inverse temperature for several chain lengths in the ERI-type silica. Over the complete temperature range (300−700 K), Arrhenius-type behavior of the form $D_\infty\, e^{-E_D/(k_BT)}$ is found. The slope of a fitted line in the figure corresponds to $-E_D$, and the value at infinite temperature is D_∞. The activation energy is related to the height of the energy barrier arising from the repulsive forces involved in penetrating the relatively small windows of the zeolite framework. The nature of the surface and the precise shape of the pore appear to be of secondary importance.[40] The precise form of the frequency factor D_∞ varies with the shape of the free energy barrier.

The activation energy for diffusion, E_D, is plotted in Figure 14a for ERI- and CHA-type silica. The simulation curve is qualitatively the inverse of the general shape of the diffusion curves, that is, if a molecule has a high mobility, the activation energy is small and vice versa. The experimental results for ERI-type zeolites are more difficult to interpret. The diffusion path of a C_{13} is still quite tortuous, and an activation energy of zero is doubtful. Measuring diffusion of C_{13} or higher accurately in ERI-type zeolites or intergrowths between ERI- and OFF-type zeolites might prove to be beyond current experimental techniques. The order of magnitude of the C_6-C_{12} range is however quite well represented by our simulation data. We find significantly higher activation energies for C_3-C_5.

In Figure 14b, the frequency factors for ERI- and CHA-type silica are shown. Gorring found a compensation effect in which the D_∞ increases as the activation energy E_D increases. The simulation results show only structural effects, and the curves are relatively straightforward to interpret. The molecules in the C_2-C_5 range have the highest orientational freedom, while for higher chain lengths, the alkane gets more and more constrained. This effect continues up to C_{10} for CHA-type silica and $C_{12}-C_{13}$ for ERI-type silica. These molecules represent local maxima. Longer molecules have to stretch through a window into two cages, leading again to more orientational freedom. We note that the maximum in the frequency factor corresponds to the minimum of the activation energy and the maximum in the diffusion constant.

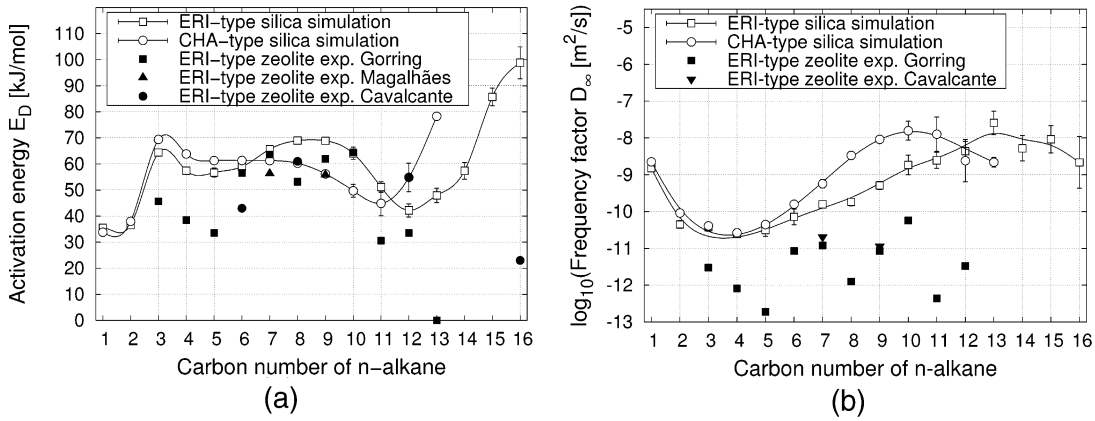

Figure 14. Fit to the Arrhenius expression for ERI- and CHA-type silica as a function of chain length: (a) activation energies in units of kJ/mol; (b) logarithm of the frequency factors D_∞ in units of m^2/s. The simulation results are compared to the experimental results obtained by Gorring,[2] Cavalcante et al.,[12] and Magalhães et al.[13] Error bars on the simulation data are only shown when larger than the symbol size.

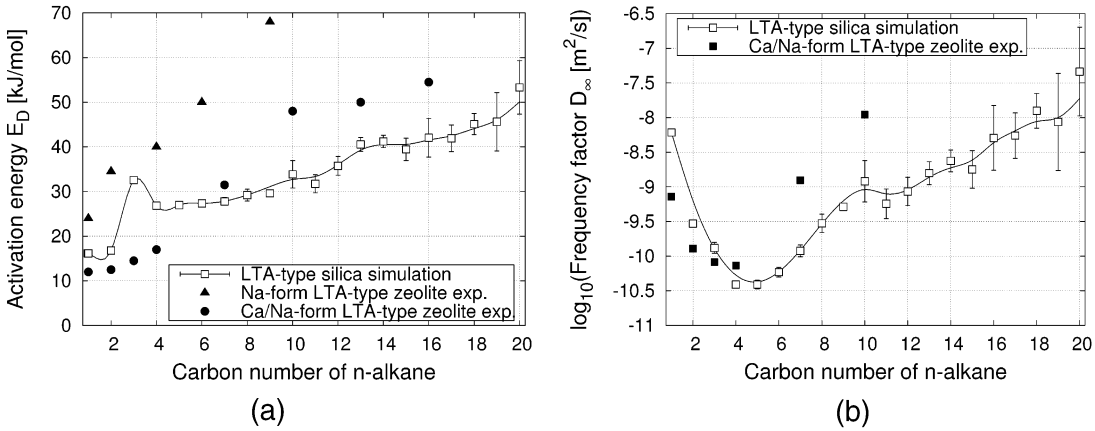

Figure 15. Fit to the Arrhenius expressions for LTA-type silica as a function of chain length: (a) activation energies in units of kJ/mol; (b) logarithm of the frequency factors D_∞ in units of m^2/s. The results are compared to the experimental results obtained by Eic and Ruthven[39] and data published in ref 40. Error bars on the simulation data are only shown when larger than the symbol size.

In Figure 15a, the activation energy obtained for LTA-type silica from simulation is plotted, along with experimental results for the Na and Ca/Na forms of LTA-type zeolites from refs 39 and 40. For a given chain length, the activation energy for diffusion in the Na form of LTA-type zeolites is higher than that for the Ca/Na form, reflecting their difference in the pore size. We were unable to find data on the all-silica version of the LTA-type zeolite, but despite this, the qualitative agreement with the Ca/Na form of the LTA-type zeolite is already reasonable, and agreement with a cation-free LTA-type sieve is expected to be quantitatively better. Figure 15b shows the frequency factors. Both datasets suggest that C_4-C_5 has the most orientational freedom and lead to the lowest attempt frequency. Unlike ERI- and CHA-type silica, LTA-type silica exhibits a compensation effect, that is, the activation energy increases, and the frequency factor increases concomitantly. The former increases because the higher mobility that comes with an increase in temperature impedes diffusion through a window; the latter increases because the same mobility results in more attempts to pass through the window. Apparently these effects cancel out each other.

We note that the LTA-type cavities are large enough to contain molecules up to C_{23}. They can bend, fold, or coil like a spring. In addition to intercage entropic barriers (i.e., windows), also intracage entropic energy barriers can be present. For lower temperatures, the temperature dependence of the frequency factor becomes important. It has been shown in simulations on ethane molecules that at low temperatures (150−300 K) diffusion can even decrease with increasing temperatures because heating the system moves the molecule away from the window, increasing the entropic barrier for cage-to-cage motion.[41]

D. Free Energy Profiles. The Henry coefficient can be considered as a spatial average of the free energy over the complete zeolite space (see eq 10). In simulations, we are able to extract more detailed information such as the free energy of a molecule as a function of position. This is not an easily obtainable quantity in experiments. In addition to the potential energy, the free energy $F(q)$ also contains an entropy contribution and is directly related to the probability of the molecule to be found at position q (see eq 16). We have plotted the free energy profiles (spline fits) at 600 K in erionite in units of k_BT for C_1-C_5 and C_8 in Figure 16. The description as an activated process is well justified because $\Delta F \gg k_BT$.

The free energy difference of ERI- (Figure 17a), CHA- (Figure 17b), and LTA-type silica (Figure 17c) can be analyzed

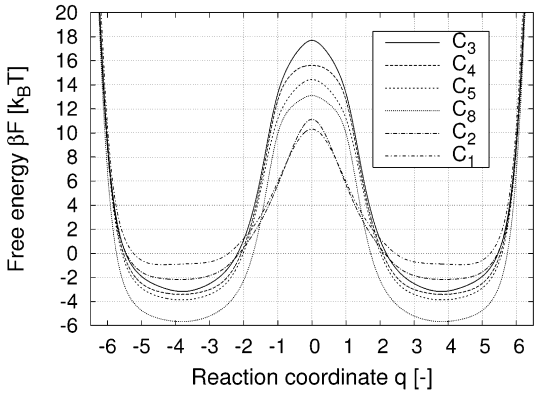

Figure 16. Free energy profiles for C_1-C_5 and C_8 in ERI-type silica in units of k_BT as a function of the dimensionless reaction coordinate q (lines from top to bottom at $q = 0$ in order of the legend). The 8T-ring window corresponds to $q = 0$, $q \approx -4$ corresponds to a location deep inside cage A, and $q \approx 4$ corresponds to a location deep inside cage B.

in terms of the value inside the cage and the value at the barrier. The simulations show that the dominating contribution to the diffusion coefficient is the height of the free energy barrier associated with the window between the cages. This height is given by the free energy difference between a molecule positioned in the cage and a molecule on top of the barrier. The depth of the free energy is directly related to the Henry coefficients. For the molecules in the cage, we observe that as we increase the chain length the minimum of the free energy decreases until we reach an optimal chain length beyond which the *n*-alkanes no longer fit comfortably in one cage. For chain lengths longer than this optimal length, the free energy increases rapidly until the molecule is so big that additional atoms are added comfortably in the second cage and the minimum free energy is decreasing again. For the free energy of a molecule on top of the barrier, we observe an increase from C_1 to C_3 as more atoms are placed on top of the barrier. For C_3, all atoms feel the influence of the window. Any additional atom will be placed in more favorable positions outside the window, and therefore, the barrier decreases for *n*-C_4 and continues to decrease until the molecule is so large that it feels the limitations of the cage. Beyond this chain length, the maximum of the free energy increases rapidly. Combining these effects gives the generic diffusion behavior as a nonmonotonic function of chain length: first a decrease followed by a possible plateau, an increase, and finally a decrease again. Key parameters in this mechanism are the presence of a narrow window combined with

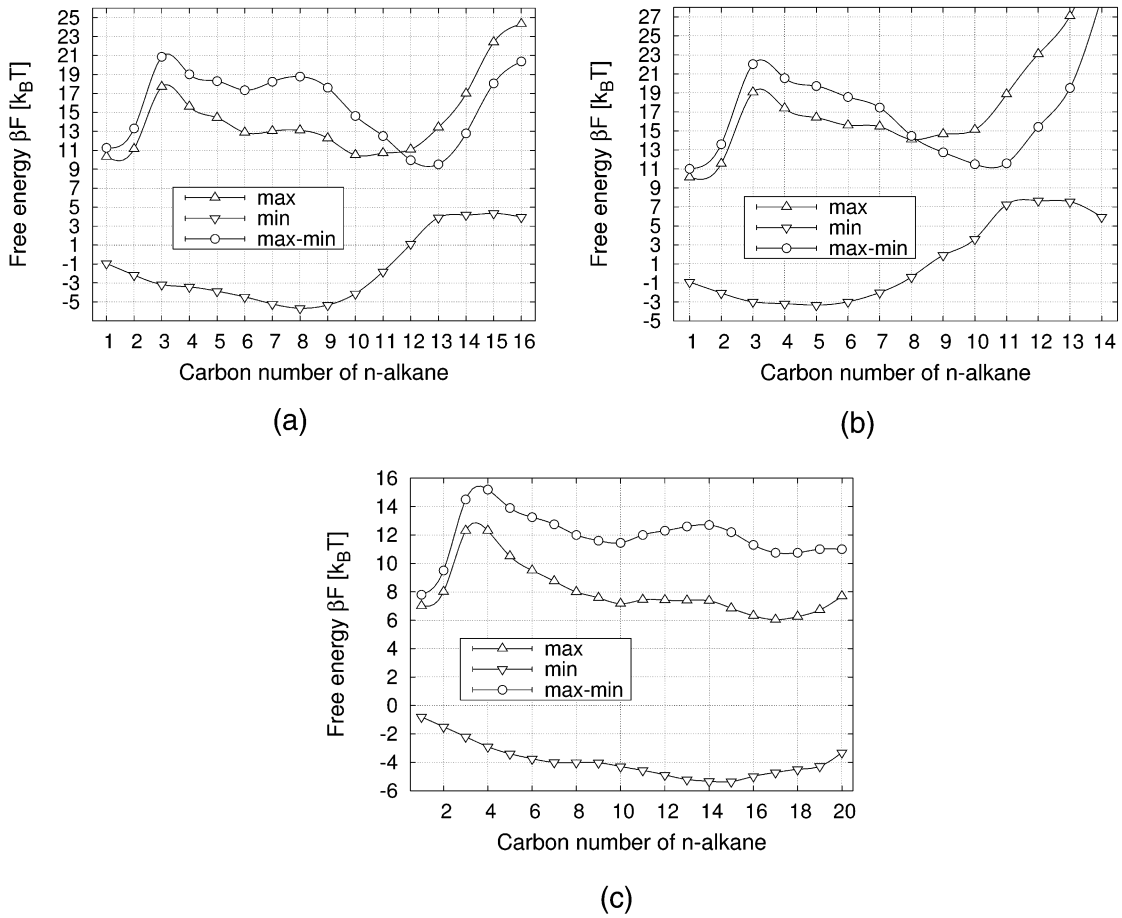

Figure 17. The free energy maximum, minimum, and difference between maximum and minimum in units of k_BT for (a) ERI-type silica, (b) CHA-type silica, and (c) LTA-type silica at 600 K.

a cage structure. By optimizing the effective cage size, one can shift the location of the second maximum to a desired value.

VII. The Window Effect Reexamined

The idea of adsorption on a periodic substrate that forms periodic arrays that are either commensurate or incommensurate with the substrate originates from the 1938 Frenkel−Kontorowa (FK) model.[7,8,42] The adsorbed atoms at positions x_n are treated as a harmonic chain with equilibrium lattice spacing a. The substrate is a one-dimensional periodic lattice with period b. The interaction between the nth adsorbed atom and the periodic substrate is described by a potential energy, $V(x_n)$. The model contains a "floating phase" in which the equilibrium lattice spacing a of the adsorbed lattice can be an arbitrary multiple of the substrate periodicity b. The diffusion and thermodynamic characteristics of molecules of which the shape is commensurate with that of the zeolite pore is very different from those of the incommensurate ones. It has been demonstrated that molecular sieves favor the formation of reaction intermediates that have a shape commensurate with their pore shape.[43]

The similar models of Nitsche and Wei[11] and Ruckenstein and Lee[9] use stiff rods to model *n*-alkanes. Due to the simplifications, the model cannot predict the location of the maximum, nor can it describe the intracage behavior correctly, that is, the minima. The entropy effect (there is variety of conformations depending on the structure of the adsorbate) has been ignored, and only a one-dimensional diffusion path is taken into account. Despite these simplifications, they corroborate the essence of the window effect: a stochastic motion through a regular array of potential barriers. An earlier proposed model by Derouane et al.[10] analyzed Gorring's results in terms of energy and surface curvature effects by applying a segmentational diffusion principle, that is, a translation occurs by successive segmental displacements. All segments are affected by different free energy environments. The model includes two distinct trapping cases: a portion of the molecule lying in the cage and the remaining portion lying in the interconnecting window space or the opposite filling order. For the sake of simplicity, the probability of the cases is equally weighted. In contrast to the other models, the authors attribute the changes in the diffusivity to a variation in the sticking force. Because of the distinction between a cage and window region, this model captures the physics of the intracage behavior somewhat better than the rod models.

Tsekov and Smirniotis[44] extended the concept of resonance diffusion by Ruckenstein and Lee[9] to include the effect of the zeolite structure and the alkane vibrations. Because the mechanics of crossing channels is hard to describe with a theoretical model, it is again restricted to channel-type zeolites such as those with LTL-type structure. They demonstrate that the existence of a sequence of expansions and apertures alone is not enough. The energy barrier should be sufficiently high to observe the diffusion peaks. Talu et al.[45] found experimental evidence of a resonance diffusion effect in silicalite. Their results obtained by steady-state single-crystal membrane technique agreed well with the MD results of Runnenbaum and Maginn.[46] In the latter report, it has been suggested that although resonance diffusion is a real effect in zeolite, it will only occur under special conditions: low temperature, rigid sorbate, smooth channels, and low loadings. The acceleration of the diffusion

rate due to resonance effects does not exceed a factor of 2. Therefore, the authors attribute the more dramatic acceleration reported by Gorring to other effects.

It is important to note that in our approach *all* possible configurations (translations, rotations, and internal configurational changes) and as a consequence *all* possible diffusion paths through the zeolite are represented with the proper weight. As such, the techniques can be straightforwardly applied to other cage/window-type zeolites. The heats of adsorption and the Henry coefficients shed light on a possible window effect before computing the more computationally demanding diffusion coefficients at interesting chain lengths.

We would like to comment on the positions and total amount of the cations within the zeolite structure and of their relevance for the obtained results. The available experimental data on zeolites with window effects is contradictory and very scattered. There exists systematic data for *n*-alkanes up to C_{14} on potassium-exchanged OFF/ERI intergrowths,[2] for ones up to C_{12} on proton-exchanged CHA-type zeolites,[3] and for a few selected alkanes on various types of ERI/OFF intergrowths by Cavalcante et al.[12] and Magalhães et al.[13] Lattice intergrowths and defects, cations, and associated aluminum atoms create strong disorder, increase the hopping activation energy, inhibit the mobility of sorbates, and slow the diffusion process. Factors such as the existence of several different energetically favorable cation sites complicate the diffusion process. In addition, our Henry coefficients indicate abnormally low adsorption in ERI- and CHA-type zeolites for chain lengths close to or longer than the cage size.

The positions of ions are of critical importance if they are located in the windows obstructing the diffusion. The difference between the Na form of the LTA-type zeolite and the Ca/Na form is a striking example.[40] The Ca/Na form (zeolite 5A) has four calcium and four sodium ions per cage. None of the windows is blocked by an ion, and the free diameter of the windows is 5 Å. The Na form (zeolite 4A) contains 12 sodiums per cage, and 100% of the windows are occupied with an ion, reducing the effective window size to 4 Å. Exchange with potassium would reduce the window size to 3 Å (zeolite 3A). The difference in diffusion is large: the coefficients in 4A are 4 orders of magnitude lower than that in 5A. The Ca form of CHA-type zeolite is another example in which the ions are located in the windows.[47] However, the positions are dependent on pretreatment of the zeolite sample (the dehydration steaming process).

Although the locations of protons can potentially be determined by neutron diffraction in an empty zeolite, they are easily displaced by diffusing adsorbates, and considering their small size, the impediment of diffusion is expected to be small. In accordance with this view, our all-silica CHA-type zeolite results agree well with the H−CHA experimental results, although a quantitative comparison is difficult because of the unknown crystal size in the experiment. We note that the original cracking data of Chen was performed using H−ERI. The actual samples used by Gorring[2], Cavalcante et al.,[12] and Magalhães et al. were rather different in composition of cations and intergrowth ratio. However, in some forms of the ERI-type zeolite[48] and the Ca/Na form of the LTA-type zeolite,[40] the ions are known to be located in the cages and not in the windows. Hence, they are expected to have a somewhat better adsorption inside the cage (Henry coefficients), but the maximum of the free energy at the windows may be virtually unchanged. Therefore, the order of magnitude difference in diffusion could possibly also be found in some of the cation-loaded versions of ERI-type zeolite.

To unambiguously detect the window effect in reality is by far no trivial task, both in view of the requirements for the experimental techniques and the quality of the nanoporous materials. In view of the difficulties, it would be of high interest to the simulation community to experimentally validate the diffusion behavior of alkanes as a function of chain length in ERI-, CHA-, and LTA-type silica or their aluminum phosphate analogues (viz., AlPO-17,[49] AlPO-34, and SAPO-42, respectively). We note that recently an all-silica form of the CHA-type zeolite has been synthesized.[50]

VIII. Conclusions

We studied the effect of the zeolite structure on the diffusion of *n*-alkanes as a function of carbon number. The ERI-, CHA-, and LTA-type frameworks consist of cages separated by small windows but differ in the size and shape of the cages and in the orientation of the windows with respect to the cage. In contrast to channel zeolites such as the OFF-type, the cage/window-type zeolites showed a cage effect for adsorption and diffusion: a nonmonotonic, periodic dependence of the Henry coefficients, heats of adsorption, and diffusion coefficients on the chain length. The simulations corroborate the existence of the window effect in ERI- and CHA-type silica with the positions of the minima and maxima determined by size and orientational crystal parameters. When a molecule is incommensurate with the cage structure, the diffusion rate increases by orders of magnitude. The corresponding chain length is the maximum length at which a molecule still fits in a single cage: C_{13} for ERI-type silica, C_{11} for CHA-type silica, and C_{23} for LTA-type silica. These crossover points are directly related to the local minima in the Henry coefficients, the heats of adsorption, and the activation energies and to the local maxima in the diffusion coefficients and the frequency factors. In the controversy about the experimental results, we side with Gorring, who was the first and only to report experimental data indicating the "window effect". This opens the possibility of length selective cracking, where the length distribution is controlled by choosing structures with the appropriate cage size.

Acknowledgment. We thank T. L. M. Maesen, S. Calero, R. Krishna, T. Vlugt, P. Bolhuis, E. J. Meijer, T. van Erp, M. Schenk, and D. Frenkel for valuable discussions, suggestions, and comments on our manuscript. The investigations are supported in part by the Netherlands Research Council for Chemical Sciences (CW).

Note Added after ASAP Posting

This article was released ASAP on 10/11/2003 with errors in the *y*-axis of Figure 7b and in the descriptions of the ERI- and CHA-type cages. The correct version was posted on 10/21/2003.

References and Notes

(1) Chen, N. Y.; Maziuk, J.; Schwartz, A. B.; Weisz, P. B. *Oil Gas J.* **1968**, *66*, 154−157.

(2) Gorring, R. L. *J. Catal.* **1973**, *31*, 13−26.

(3) Chen, N. Y.; Garwood, W. E.; Dwyer, F. G. *Shape selective Catalysis in industrial Applications*, 2nd edition, revised and expanded; Chemical Industries: New York, 1996.

(4) Chen, N. Y.; Lucki, S. J.; Mower, E. B. *J. Catal.* **1969**, *13*, 329−332.

(5) Dubbeldam, D.; Calero, S.; Maesen, T. L. M.; Smit, B. *Phys. Rev. Lett.* **2003**, *90*, 245901.

(6) Dubbeldam, D.; Calero, S.; Maesen, T. L. M.; Smit, B. *Angew. Chem., Int. Ed.* **2003**, *42*, 3624−3626.

(7) Frenkel, Y. I.; Kontorowa, T. *Phys. Z. Sowjetunion* **1938**, *13*, 1.

(8) Kontorowa, T.; Frenkel, Y. I. *Zh. Eksp. Teor. Fiz.* **1938a,b**, *8*, 89, 1340.
(9) Ruckenstein, E.; Lee, P. S. *Phys. Lett. A* **1976**, *56*, 423−424.
(10) Derouane, E. G.; Andre, J. M.; Lucas, A. A. *J. Catal.* **1988**, *110*, 58−73.
(11) Nitsche, J. M.; Wei, J. *J. AlChe.* **1991**, *37*, 661−670.
(12) Cavalcante, C. L., Jr.; Eić, M.; Ruthven, D. M.; Occelli, M. L. *Zeolites* **1995**, *15*, 293−307.
(13) Magalhães, F. D.; Laurence, R. L.; Conner, W. C. *J. AlChe.* **1996**, *42*−*86*, 68.
(14) Chandler, D. *J. Chem. Phys* **1978**, *68*, 2959.
(15) Bennett, C. H. In *Diffusion in Solids: Recent Developments*; Nowick, A. S., Burton, J. J., Eds.; Academic Press; New York, 1975; pp 73−113.
(16) Ruiz-Montero, M. J.; Frenkel, D.; Brey, J. J. *Mol. Phys.* **1996**, *90*, 925−941.
(17) Ryckaert, J. P.; Bellemans, A. *Faraday Dicuss. Chem. Soc.* **1978**, *66*, 95−106.
(18) Ryckaert, J. P.; Bellemans, A. *Chem. Phys. Lett.* **1975**, *30*, 123−106.
(19) Bezus, A. G.; Kiselev, A. V.; Lopatkin, A. A.; Du, P. Q. J. *J. Chem. Soc., Faraday Trans. 2* **1978**, *74*, 367−379.
(20) Vlugt, T.; Krishna, R.; Smit, B. *J. Phys. Chem. B* **1999**, *103*, 1102−1118.
(21) Maesen, T. L. M.; Schenk, M.; Vlugt, T. J. H.; de Jonge, J. P.; Smit, B. *J. Catal.* **1999**, *188*, 403−412.
(22) IZA Structure Commission. Database of Zeolite Structures. http://www.iza-structure.org/databases/ (accessed May 2003).
(23) Demontis, P.; Suffritti, G. B.; Fois, E. S.; Quartieri, S. *J. Phys. Chem.* **1992**, *96*, 1482−1490.
(24) Fritzche, S.; Wolfsberg, M.; Haberlandt, R.; Demontis, P.; Suffritti, G. B.; Tilocca, A. *Chem. Phys. Lett.* **1998**, *296*, 253.
(25) Vlugt, T. J. H.; Schenk, M. *J. Phys. Chem. B* **2002**, *106*, 12757−12763.
(26) Frenkel, D.; Smit, B. *Understanding molecular simulation*, 2nd ed.; Academic Press: London, 2002.
(27) Smit, B.; Siepmann, J. I. *J. Phys. Chem.* **1994**, *98*, 8442−8452.
(28) Rosenbluth, M.; Rosenbluth, A. *J. Chem. Phys.* **1955**, *23*, 356−359.
(29) Smit, B.; Daniël, L.; Loyens, J. C.; Verbist, G. L. M. M. *Faraday Dicuss. Chem. Soc.* **1997**, *106*, 93−104.
(30) Press, W. H.; Flannery, B. P.; Teukolsky, S. A.; Vetterling, W. T. *Numerical Recipes in C*; Cambridge University Press: New York, 1988.
(31) Alberti, A.; Cruciani, G.; Galli, E.; Vezzalini, G. *Zeolites* **1996**, *17*, 457−461.
(32) Pluth, J. J.; Smith, J. V.; Bennett, J. M. *Acta Crystallogr.* **1986**, *C42*, 283−286.
(33) Bennet, J. M.; Gard, J. A. *Nature* **1967**, *214*, 1005−1006.
(34) Calligaris, M.; Nardin, G.; Randaccio, L. *Zeolites* **1983**, *3*, 205−208.
(35) Pluth, J. J.; Smith, J. V. *Zeolites* **1980**, *102*, 4704−4708.
(36) Schroeder, W.; Martin, K.; Lorensen, B. *The Visualization Toolkit: an object-oriented approach to 3D graphics*; Prentice-Hall: Upper Saddle River, NJ, 1996.
(37) The Visualization Toolkit. http://public.kitware.com/VTK/ (accessed May 2003).
(38) Ruthven, D. M.; Kaul, B. K. *Adsorption* **1998**, *4*, 269−273.
(39) Eic, M.; Ruthven, D. M. *Zeolites* **1988**, *8*, 472−479.
(40) Kaerger, J.; Ruthven, D. M. *Diffusion in Zeolites and other microporous solids*; John Wiley & Sons: New York, 1992.
(41) Schüring, A.; Auerbach, S. M.; Fritzsche, S.; Haberlandt, R. *J. Chem. Phys.* **2002**, *116*, 10890−10894.
(42) Braun, O. M.; Kivshar, Y. *Phys. Rep.* **1998**, *306*, 1−108.
(43) Schenk, M.; Smit, B.; Vlugt, T. J. H.; Maesen, T. L. M. *Angew. Chem., Int. Ed.* **2001**, *40*, 736−739.
(44) Tsekov, R.; Smirniotis, P. G. *J. Phys. Chem. B* **1998**, *102*, 9385−9391.
(45) Talu, O.; Sun, M. S.; Shah, D. B. *J. AlChe.* **1998**, *44*, 681−694.
(46) Runnebaum, R. C.; Maginn, E. J. *J. Phys. Chem. B* **1997**, *101*, 6394−6408.
(47) Grey, T.; Gale, J.; Nicholson, D.; Peterson, B. *Microporous Mesoporous Mater.* **1999**, *31*, 45−59.
(48) Alberti, A.; Martucci, A.; Galli, E.; Vezzalini, G. *Zeolites* **1997**, *19*, 349−352.
(49) Pluth, J. J.; Smith, J. V. *Acta Crystallogr.* **1986**, *42*, 283−286.
(50) Díaz-Cabanas, M.-J.; Barrett, P. A.; Camblor, M. A. *Chem. Commun.* **1998**, *17*, 1881−1882.